Data S1.

Image acquisition of PET/CT. 18F-FDG PET/CT images were taken according to a standard protocol. Patients were fasted for at least 6 h and their pre-injection blood glucose levels were below 160 mg/dl (7.8 mmol/l). Sixty minutes after the injection of 18F-FDG (dose 0.14 mCi/kg), imaging was performed on a PET/CT scanner (Discovery STE; GE Healthcare) with a 700 mm FOV and a slice thickness of 3.27 mm. Three-dimensional (3D) data acquisition was performed for 3 min per bed position, which was followed by imaging reconstruction with the 3D-ordered subset expectation maximization method. Correction of segmented attenuation was performed using CT (140 kV, 120-240 mAs) to produce 128x128 matrix images. The CT images were reconstructed using a conventional filtered back-projection method. The intrinsic system sensitivity was 8.5 cps/kBq for 3D acquisition. Patients were scanned from the thigh to the head in the arms-down position.

Image acquisition of MR imaging. Established MR imaging protocols include T1-weighted turbo spin echo, T2-weighted turbo spin echo and fat suppression T2 turbo inversion recovery magnitude (TIRM). The sequence parameters (repetition time/echo time) used for the spine were as follows: 537/8.8 for T1-weighted images; 3,600/101 for T2-weighted images; 4,200/50 for T2 TIRM; FOV, 320 mm; slice thickness, 4 mm; slices, 11; and orientation, sagittal. The examinations were performed with a 1.5T MR imaging system (Magnetom Avanto; Siemens Medical Solutions) using a body matrix coil.

Image interpretation criterion. Visual analysis for myeloma bone disease was performed by evaluating the transaxial and sagittal images of the patients separately for each applied modality by two nuclear medicine physicians and two radiologists. The imaging manifestations of MM disease can present as FLs, DI, extra-medullary disease (EMD), or mixture of them. FLs are circumscriptive lesions > 5 mm in diameter to avoid excessive false positivesz 1), which present on intra-axial (spine and sacral bone) or extra-axial locations; paramedullary disease (PMD), bone lesions involving the surrounding soft tissues with bone cortical interruption, also sort into this category. DI can present as homogeneous, heterogeneous or variegated, also known as 'salt and pepper' (S&P), and may be divided into three grades to apply the D-S PLUS staging system: Mild, moderate and severe. EMD grows exclusively in the soft tissues independent of the bone marrow and involves nodal sites (including cervical, supraclavicular, mediastinal, axillary, retroperitoneal, mesenteric and inguinal nodal sites) and extranodal sites (including liver, muscle, spleen and skin). Differentiating a true EMD from PMD is important because the prognostic profile varies between the two presentations, with EMD having a worse prognosis (2).

MR imaging. Adult bone marrow is predominantly composed of fat, which increases with age (3). The signal intensities on MR imaging are based on the proportionate composition of red and yellow marrow and to a lesser extent mineralized matrix (4-6). Bone marrow with a hyperintense signal compared with the disk on T1-weighted images (T1wi) and an isointense or hypointense signal compared with the subcutaneous fat on T2-weighted images (T2wi) were regarded as normal (Fig. S1) (4). Notably, FLs are hypointense on T1wi and hyperintense on T2wi on MR imaging. Furthermore, FLs are hyperintense on T2 fat-suppressed images because of the high amount of neoplastic cells and water in the lesions (Fig. 1) (4,7).

In the present study, the DI grades were classified according to Baur and Staebler. Normal/mild DI of the bone marrow was previously defined (Fig. S1) (8,9). Moderate DI was defined as a decrease in the T1wi signal intensity of the bone marrow, which was still higher when compared with the signal of the intervertebral discs. A decrease of the signal intensity as low as that of the intervertebral discs (or even lower) on the T1wi was graded as severe DI (Fig. S2). Although the S&P pattern was patchy on T1wi, no FLs were observed on TIRM (Fig. S3), which has been associated with lower disease burden and is usually classified as stage I disease (10).

PET/CT. The criteria interpretation of PET/CT was based on a visual assessment. We avoided a semi-quantitative readout for PET scan interpretation because even a low Standardized Uptake Value variability of different PET centers could generate inconsistent interpretations in borderline cases when a given semi-quantitative positivity cut-off was set, which would have produced results that were not comparable and not reproducible (5,11).

However, semi-quantitative data were also collected in the reference organ (liver) and target organ (bone marrow) to determine the different DI patterns. The liver 18F-FDG uptake was measured using a circular region of interest (ROI) with a radius >3 cm in the central portion of the liver far away from its edge. The bone marrow 18F-FDG uptake was quantified using three ROIs of similar sizes drawn on the medullary component of L3-L5 vertebral bodies, using CT images as location references. For the PET component of the PET/CT scan, positive DI was defined when bone marrow uptake was > liver +10%, and it was subdivided as moderate and severe when DI bounded by uptake was more than twice that of the liver; otherwise, it was considered negative (12). For the CT component of the PET/CT scan, positive DI was defined when diffuse bone destruction was present, which had been discussed detailed in the main body. The DI pattern of PET/CT could present various combinations of PET and CT as follows: Both CT and PET positive DI; both CT and PET negative DI; and one of CT or PET positive DI with the other negative DI.

FLs were defined as lesions that had more intense 18F-FDG uptake compared with physiologic bone marrow (in the lumbar spine and/or pelvis) and/or physiologic liver (no known liver disease, hepatitis or cirrhosis and so on), with or without a corresponding CT finding, or osteolytic lesions on CT with low or no 18F-FDG uptake (7,9,12).

References

1. Walker R, Barlogie B, Haessler J, Tricot G, Anaissie E, Shaughnessy JD Jr, Epstein J, van Hemert R, Erdem E, Hoering A, *et al*: Magnetic resonance imaging in multiple myeloma: Diagnostic and clinical implications. J Clin Oncol 25: 1121-1128, 2007.

2. Walker RC, Brown TL, Jones-Jackson LB, De Blanche L and Bartel T: Imaging of multiple myeloma and related plasma cell dyscrasias. J Nucl Med 53: 1091-1101, 2012.
3. Howe BM, Johnson GB and Wenger DE: Current concepts in MRI of focal and diffuse malignancy of bone marrow. Semin Musculoskelet Radiol 17: 137-144, 2013.
4. Silva JR Jr, Hayashi D, Yonenaga T, Fukuda K, Genant HK, Lin C, Rahmouni A and Guermazi A: MRI of bone marrow abnormalities in hematological malignancies. Diagn Interv Radiol 19: 393-399, 2013.
5. Vande Berg BC, Malghem J, Lecouvet FE and Maldague B: Magnetic resonance imaging of the normal bone marrow. Skeletal Radiol 27: 471-483, 1998.
6. Dimopoulos M, Terpos E, Comenzo RL, Tosi P, Beksac M, Sezer O, Siegel D, Lokhorst H, Kumar S, Rajkumar SV, *et al*; IMWG: International myeloma working group consensus statement and guidelines regarding the current role of imaging techniques in the diagnosis and monitoring of multiple Myeloma. Leukemia 23: 1545-1556, 2009.
7. Dutoit JC, Vanderkerken MA, Anthonissen J, Dochy F and Verstraete KL: The diagnostic value of SE MRI and DWI of the spine in patients with monoclonal gammopathy of undetermined significance, smouldering myeloma and multiple myeloma. Eur Radiol 24: 2754-2765, 2014.
8. Stäbler A, Baur A, Bartl R, Munker R, Lamerz R and Reiser MF: Contrast enhancement and quantitative signal analysis in MR imaging of multiple myeloma: Assessment of focal and diffuse growth patterns in marrow correlated with biopsies and survival rates. AJR Am J Roentgenol 167: 1029-1036, 1996.
9. Baur A, Stäbler A, Nagel D, Lamerz R, Bartl R, Hiller E, Wendtner C, Bachner F and Reiser M: Magnetic resonance imaging as a supplement for the clinical staging system of Durie and Salmon? Cancer 95: 1334-1345, 2002.
10. Baur-Melnyk A, Buhmann S, Dürr HR and Reiser M: Role of MRI for the diagnosis and prognosis of multiple myeloma. Eur J Radiol 55: 56-63, 2005.
11. Chauvie S, Biggi A, Stancu A, Cerello P, Cavallo A, Fallanca F, Ficola U, Gregianin M, Guerra UP, Chiaravalloti A, *et al*: WIDEN: A tool for medical image management in multicenter clinical trials. Clin Trials 11: 355-361, 2014.
12. Nanni C, Zamagni E, Versari A, Chauvie S, Bianchi A, Rensi M, Bellò M, Rambaldi I, Gallamini A, Patriarca F, *et al*: Image interpretation criteria for FDG PET/CT in multiple myeloma: A new proposal from an Italian expert panel. IMPeTUs (Italian Myeloma criteria for PET USe). Eur J Nucl Med Mol Imaging 43: 414-421, 2016.

Figure S1. (A and B) Normal pattern of the bone marrow in a 77-year-old man. (A) T1wi indicated a hyperintense signal compared with the intervertebral disk. (B) T2wi revealed the hyperintense signal caused yellow bone marrow. (C and D) FLs in the first lumbar vertebral body of a 64-year-old man. (C) T1wi indicated a hypointense signal, and (D) T2-TIRM revealed a hyperintense signal. FL, focal lesions.

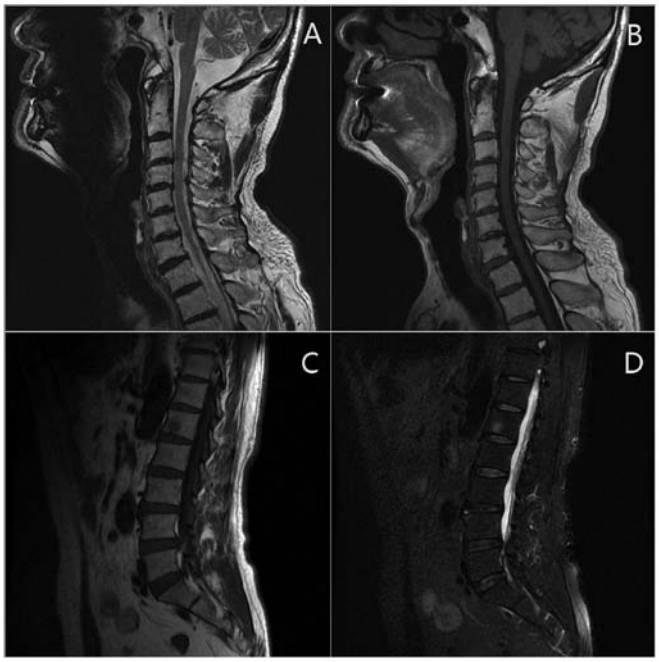

Figure S2. A 65-year-old male with severe DI. (A) T1wi indicated a decreased signal, which was as low as that of the intervertebral discs. (B) T2-TIRM revealed a hyperintense signal compared with muscle.

Figure S3. A 64-year-old male with the S&P pattern. (A) T1wi showed mixed hyper- and hypointense, also known as a S&P pattern. (B) On T2-TIRM images no focal lesions were identified, this finding corresponds to normal bone marrow. A T12 vertebral body compression fracture was indicated.